RESEARCH ARTICLE

Key Points:
- Model reveals spatial variability in seasonality of nitrous oxide emissions driven by differences in stratification intensity and duration
- The northwest European shelf contributes between 3.3% and 6.8% to total nitrous oxide emissions from European shelves and estuaries
- Total amount of nitrous oxide is controlled by ammonium availability; changes in nutrient input can alter regional emissions

Supporting Information:
- Supporting Information S1
- Figure S1
- Figure S2

Correspondence to:
G. Lessin,
gle@pml.ac.uk

Modeling the Seasonality and Controls of Nitrous Oxide Emissions on the Northwest European Continental Shelf

Gennadi Lessin[1] (ID), Luca Polimene[1] (ID), Yuri Artioli[1] (ID), Momme Butenschön[2] (ID), Darren R. Clark[1] (ID), Ian Brown[1] (ID), and Andrew P. Rees[1] (ID)

[1]Plymouth Marine Laboratory, Plymouth, UK, [2]Euro-Mediterranean Center on Climate Change (CMCC), Bologna, Italy

Abstract Estimates of oceanic emissions of nitrous oxide (N_2O) are surrounded by a considerable degree of uncertainty, particularly regarding the contribution of productive shelf regions, where assessments are based on limited observations. In this paper, we have applied a coupled hydrodynamic-biogeochemical model resolving N_2O dynamics to estimate N_2O emissions within the northwest European continental shelf. Based on 10-year average distributions (2006–2015), dominant seasonal patterns of N_2O air-sea exchange were identified. Within the southwest region of the shelf and deep parts of the North Sea, emissions are highest during winter. Peak emissions during late autumn are typical for the northwest part of the shelf and central North Sea, while in the western English Channel, Irish Sea and western North Sea peak outflux shifts toward early autumn. Within these regions, most N_2O production occurs below the seasonal pycnocline, and duration and intensity of stratification defines the timing and rate of its subsequent release to the atmosphere. In contrast, within the southeast North Sea and most of the coastal areas, lack of stratification allows the excess N_2O to outgas as soon as it is produced, driven by ammonium availability, resulting in peak emissions in summer. We estimate that N_2O emissions from the northwest European shelf contribute 0.02224 Tg N to the atmosphere annually, that is, between 3.3–6.8% of total emissions from European shelves and estuaries.

1. Introduction

Nitrous oxide (N_2O) is the third most important long-lived greenhouse gas contributing ~6% of the direct anthropogenic radiative forcing, preceded by carbon dioxide and methane which contribute ~76% and ~16%, respectively (IPCC, 2013). With a global warming potential about 300 times higher than that of carbon dioxide, N_2O plays a significant role in the greenhouse effect (Myhre et al., 2013). N_2O also contributes to the destruction of stratospheric ozone (Andreae & Crutzen, 1997; Nevison & Holland, 1997), its emissions currently having the largest ozone depletion potential of all ozone depleting substances (Carpenter et al., 2014; Ravishankara et al., 2009).

The main pathways for natural N_2O emissions to the atmosphere are production during microbially mediated nitrification and denitrification processes within soils and in the ocean. During nitrification, N_2O is produced as a by-product of ammonium oxidation to hydroxylamine, or via nitrite reduction, with enhanced yield at oxygen-limited conditions (Capone, 1991; Goreau et al., 1980; Löscher et al., 2012). N_2O is also an intermediate product of denitrification, leading to either net production or net consumption flux depending on oxygen conditions (Bianchi et al., 2012; Cohen & Gordon, 1978; Nevison et al., 2003).

The ocean is an important source of N_2O to the atmosphere. According to the Fifth Assessment Report of Intergovernmental Panel on Climate Change, in 2006 mean total emissions of N_2O to the atmosphere from all natural and anthropogenic sources combined were 17.9 Tg N yr^{-1}, of which oceans contributed 21.2% (3.8 Tg N yr^{-1}), while 3.4% (0.6 Tg N yr^{-1}) originated from coastal areas including estuaries and rivers. However, these estimates are surrounded by a considerable degree of uncertainty with ranges of global, oceanic, and coastal emissions between 8.1–30.7, 1.8–9.4, and 0.1–2.9 Tg N yr^{-1}, respectively (Ciais et al., 2013). Bange et al. (1996) suggested that coastal and upwelling regions which are known for high N_2O production were

Butenschön, Darren R. Clark, Ian Brown, Andrew P. Rees

Methodology: Gennadi Lessin, Luca Polimene, Yuri Artioli, Momme Butenschön, Darren R. Clark, Ian Brown, Andrew P. Rees
Resources: Ian Brown, Andrew P. Rees
Software: Gennadi Lessin, Luca Polimene, Yuri Artioli, Momme Butenschön
Validation: Gennadi Lessin, Ian Brown, Andrew P. Rees
Visualization: Gennadi Lessin
Writing - original draft: Gennadi Lessin, Luca Polimene, Yuri Artioli, Momme Butenschön, Darren R. Clark, Ian Brown, Andrew P. Rees
Writing – review & editing: Gennadi Lessin, Luca Polimene, Yuri Artioli, Momme Butenschön, Darren R. Clark, Ian Brown, Andrew P. Rees

poorly represented in previous budgets and provided a revised estimate for global oceanic production rate of 4.5–7.64 Tg N yr^{-1}.

Our current ability for more accurate estimates of N_2O distributions and emissions is hindered by the lack of comprehensive, quality-controlled observations able to describe the spatial and temporal variability, especially within dynamic marginal seas and coastal areas. International intercomparison exercises, such as the one conducted by Wilson et al. (2018) will assure consistent quality control of N_2O measurements, and together with other recent international initiatives, such as the MarinE MethanE and NiTrous Oxide database (MEMENTO) (Bange et al., 2009; Kock & Bange, 2015) and the proposed N_2O Observation Network for harmonized measurements from various platforms (Bange et al., 2019) will contribute toward improved quality and spatiotemporal coverage of measurement data, essential for the reduction of uncertainties in global and regional estimates of emissions and their variability, as well as further development and validation of numerical models of N_2O.

Coupled hydrodynamic-biogeochemical models integrate our current understanding of ocean functioning, enabling the analysis, interpretation, and upscaling of available observational data, as well as predicting the response of N_2O to natural and anthropogenic stressors and changing climate. Recent modeling efforts largely focused on assessing mechanisms of N_2O production and projection of emissions at a global scale (Ji et al., 2018; Martinez-Rey et al., 2015; Suntharalingam et al., 2000; Suntharalingam & Sarmiento, 2000; Zamora & Oschlies, 2014). However, global models currently poorly represent coastal and shelf seas despite their disproportionally large role in biogeochemical cycling (Holt et al., 2017). To reduce the current uncertainties related to N_2O dynamics within coastal regions and their contribution to global emission rates, regional models with higher resolution of local hydrography and a detailed description of biogeochemistry are needed. These models can provide information highly relevant for the support of regional marine environmental policy development and management (Hyder et al., 2015). Furthermore, regional models allow the analysis of drivers controlling spatiotemporal distributions and sea-to-air fluxes of N_2O within shelf sea regions and therefore can help in the interpretation of existing data sets and inform the design of observational efforts to further improve understanding of N_2O processes and its emission estimates. To this end, we have applied a complex biogeochemical-ecological model resolving N_2O dynamics on the northwest European continental shelf, with the aim to (a) identify dominant seasonal patterns of N_2O air-sea flux and the drivers underpinning its variability, and (b) quantify the "present-day" contribution of the northwest European shelf as a source of N_2O to the atmosphere.

2. Materials and Methods

2.1. Model Description and Setup

For the purpose of our study we use the 3-D coupled hydrodynamic-biogeochemical modeling system NEMO-FABM-ERSEM configured on the Atlantic Meridional Margin (AMM7) domain, which is based on an update of Edwards et al. (2012). The geographical domain extends from 20°W to 13°E and 40°N to 65°N (Figure 1), and has a horizontal resolution of 1/15° in latitudinal and 1/9° in longitudinal direction, corresponding to ~7 km. Vertically, the model resolution was improved to 50 σ-z layers, from the original 32, and has a minimum bathymetry of 10 m. In areas of steep bathymetry change the total number of layers is decreased to reduce spurious vertical transport.

Atmospheric forcing is provided by the ERA-interim reanalysis of the European Centre for Medium-Range Weather Forecasts (Dee et al., 2011), while physical oceanic boundary conditions are taken from GLORYS reanalysis (Ferry et al., 2012). The model is initialized on 1 January 2000 with the physical and biogeochemical states from a previous long-term hindcast simulation and a homogeneous concentration of N_2O of 10.75 nmol L^{-1}, based on typical observational values for the study area. This combination of initial conditions allowed for a short 6-year spin-up period (2000–2005), with the last 10 years (2006–2015) used for the assessment of N_2O dynamics.

Formulation and parameterization of the biogeochemical-ecological model ERSEM follows that of Butenschön et al. (2016), extended with the processes of N_2O production and air-sea exchange described below, implemented within FABM—Framework for Aquatic Biogeochemical Models (Bruggeman & Bolding, 2014).
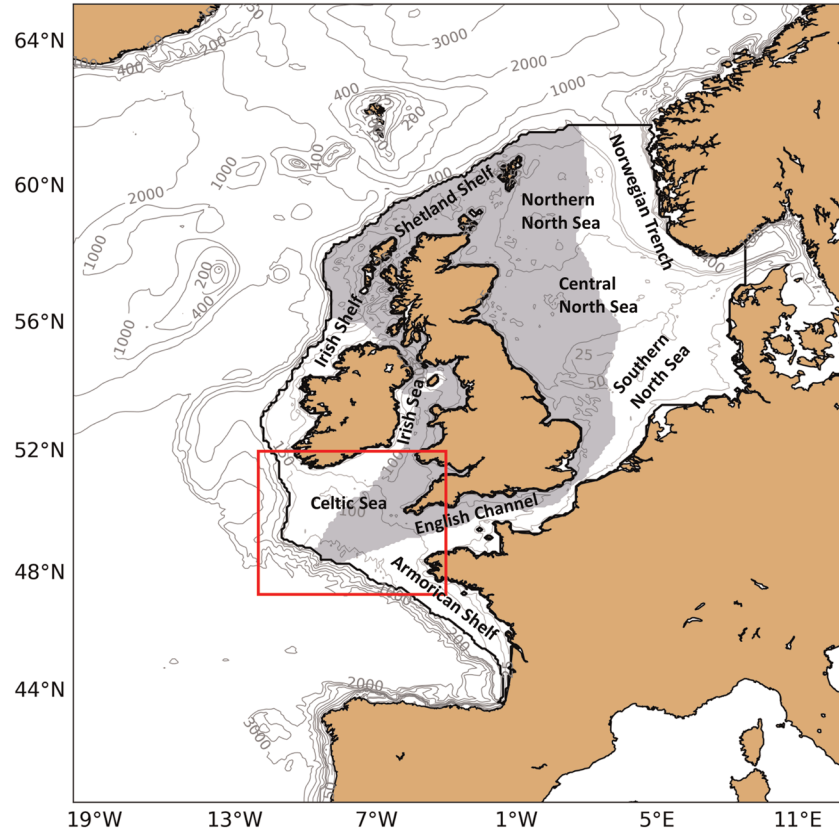
Figure 1. Map of the model domain. Black contour line outlines the northwest European continental shelf area (part of the modeled domain delineated with 200 m isobath, as well as Norwegian trench). Shaded area defines the extent of the on -shelf part of the UK Exclusive Economic Zone (EEZ). Red box delimits the mapped area shown on Figure 2, where measurements of N$_2$O were taken within the UK Shelf Sea biogeochemistry program (cruises DY018, DY029, and DY033).

In oxygenated waters N$_2$O is mainly produced as a by-product during the process of nitrification (Freing et al., 2012). Hence, the pelagic production of N$_2$O (N_2O_{prod}, nmol N L^{-1} day^{-1}) was parameterized as proportional to total nitrification flux, assuming enhancement under low oxygen conditions:

$$N_2O_{prod} = \alpha \, F_{nit} \, Enh, \tag{1}$$

where α is the N$_2$O yield constant, F_{nit} is the total nitrification flux (μmol N L^{-1} day^{-1}), and Enh is a factor enhancing N$_2$O production at low-oxygen conditions, parameterized as

$$Enh = \min\left(E_{max}, \frac{Ox^3 + h_{ox}}{Ox^3}\right), \tag{2}$$

where E_{max} is the maximum value of enhancement, Ox is the oxygen concentration (μmol O$_2$ L^{-1}) and h_{ox} is a constant. The value of E_{max} of 20 was chosen following Codispoti (2010), while h_{ox} of 2,700 (μmol L^{-3})^3 was applied.

Nitrification flux F_{nit} is modeled implicitly as a first-order process dependent on availability of ammonium (Amm) and modified by temperature, oxygen and pH:

$$F_{nit} = r_{nit} f(T) f(Ox) f(pH) Amm \tag{3}$$

Maximum ammonium mass-specific nitrification rate r_{nit} of 0.5 day^{-1} was applied. The value is rather

close to the mean specific nitrification rate of 0.55 day^{-1} reported by Yool et al. (2007) based on a wide range of measurements dominated by data from the northeast region of Atlantic Ocean.

Temperature dependency of nitrification is modeled following Blackford et al. (2004):

$$f(T) = Q_{10}^{\frac{T-10}{10}} - Q_{10}^{\frac{T-32}{3}} \tag{4}$$

where T is water temperature in degrees Celsius and Q_{10} is a coefficient of 2.0.

Dependency of nitrification on oxygen is parameterized as

$$f(Ox) = \frac{Ox^3}{Ox^3 + h_{ox}} \tag{5}$$

Finally, limitation of nitrification by pH is accounted for as

$$f(pH) = \min(2, \max(0, 0.6111pH - 3.8889)) \tag{6}$$

The formulation was parameterized by Blackford and Gilbert (2007) based on observational work of Huesemann et al. (2002).

According to Bange (2008), reported N$_2$O yields from nitrification range from 0.004% to 0.4%. Dore and Karl (1996) reported a higher yield of 0.5% for the North Pacific time series station ALOHA, while Ji et al. (2018) derived yield uncertainty range of 0.04–0.12% at oxygen concentrations above 50 μmol L^{-1}, based on measurements in the Eastern Tropical Pacific. In our model we implemented a value of 0.1% for the N$_2$O production yield at nitrification, which allowed realistic distributions of N$_2$O to be modeled on the northwest European Shelf.

Several modeling studies exclude N$_2$O production in the photic zone (e.g., Battaglia & Joos, 2018; Martinez-Rey et al., 2015) following an assumption that nitrification by ammonia-oxidizing bacteria (AOB) is inhibited by light (Horrigan & Springer, 1990; Ward et al., 1982). However, there is a growing evidence that nitrification by ammonia-oxidizing archaea (AOA) takes place within the photic zone, and that this mechanism might be the dominant route for ammonia oxidation in the upper ocean (e.g., Beman et al., 2012; Newell et al., 2013; Peng et al., 2016; Ward, 2008), although photosensitivity of AOA has also been reported (Horak et al., 2018; Merbt et al., 2012). Several studies summarized by Yool et al. (2007) (see Figure 1b therein) have shown that there is no clear increase in nitrification rate with depth, which would indicate inhibition by light in the euphotic zone. Other studies have also demonstrated nitrification to take place within the photic zone (Clark et al., 2008; Dore & Karl, 1996; Wankel et al., 2007). Moreover, experiments conducted by Smith et al. (2014) demonstrated nitrification rates in the photic zone to be more strongly regulated by competition with phytoplankton for ammonium rather than directly by light. Since details on sensitivity of nitrification to light intensity are still debated, within this work we followed the original formulation of ERSEM, where nitrification rate is not affected by light.

Pelagic denitrification-related sources and sinks of N$_2$O were not included in the present model formulation. The majority of waters within the study area are well oxygenated, and for denitrification to take place an anoxic environment is required. Therefore, we assume that the amount of denitrification occurring in the system is negligible, as was previously confirmed by in situ observations in the North Sea (Law & Owens, 1990). Furthermore, we did not include benthic sources and sinks of N$_2$O in the model formulation applied here based on the evidence that N$_2$O production rate in the North Sea sediments is very low (Law & Owens, 1990). It is likely for the major pathway of nitrogen removal in the sediments within our study area to be not denitrification, but anammox, as found by Kitidis et al. (2017) for the sediments of the Celtic Sea. The process of anammox does not involve N$_2$O production or consumption.

Air-sea flux of nitrous oxide (F_{N_2O}, μmol N$_2$O m^{-2} day^{-1}) was calculated as a product of the gas-transfer velocity k_{N_2O} and the difference between equilibrium and surface water gas concentrations:

$$F_{N_2O} = k_{N_2O} \left(N_2O_{eq} - N_2O_{sea} \right) \tag{7}$$

The gas transfer velocity was calculated following Wanninkhof (1992):

$$k_{N_2O} = 0.39 U^2 \left(\frac{Sc}{660} \right)^{-0.5}, \tag{8}$$

where U is the wind speed and Sc is the Schmidt number. Solubility of N_2O in seawater was calculated according to Weiss and Price (1980). Time-varying atmospheric partial pressure of N_2O based on monthly values over marine surface sites for the Northern Hemisphere (NOAA, 2014) was applied uniformly over the model domain.

2.2. Self-Organizing Maps

To identify dominant patterns in seasonality of N_2O air-sea exchange on the northwest European shelf we employed self-organizing map (SOM). SOM is a type of artificial neural network that uses unsupervised learning to retrieve the main underlying patterns or structures (termed nodes) within a complex data set and to produce its low-dimensional discretized representation (Kohonen, 2001). The number of SOM nodes is somewhat subjective and depends on the characteristics of input data and research questions. Following experimentation with different numbers of SOM nodes, we chose to base our implementation on four nodes organized in a linear pattern, which allowed for determination of distinct seasonal patterns of N_2O fluxes within small number of classes. Weights of each node were initialized as a linear combination of the first two principal components of the data. Thereafter, SOM was trained using all input data vectors sequentially. At the end of the training process, each node represented one of four distinct types of annual cycles of N_2O air-sea flux within the northwest European shelf. The annual cycles at each model grid point were then mapped to their closest node to define four regions with distinct seasonal pattern of N_2O fluxes. We use MiniSOM, a minimalistic NumPy based implementation of SOM (Vettigli, 2019).

2.3. Observational Data

Measurements of N_2O were made during four research cruises in the study area. These were a circumnavigation of the UK during June and July 2011 on board *RRS Discovery* (UK Ocean Acidification program cruise D366) and three cruises on board *RRS Discovery* to the Celtic Sea in November 2014, April 2015, and July 2015 (UK Shelf Sea Biogeochemistry program cruises DY018, DY029, and DY033, respectively).

A total of 181, 62, 241, and 252 samples were collected during cruises D366, DY018, DY029, and DY033, respectively. At each station, up to 10 samples were collected and analyzed at depths between the sea surface and within 10 m of the seabed. Seawaters were collected into 1 L glass bottles using acid cleaned Tygon tubing directly from CTD Niskin bottles. Samples were overfilled in order to expel air bubbles, poisoned with 200 µl of saturated $HgCl_2$ solution and temperature equilibrated at 25.0 ± 0.5 °C. In all cases samples were analyzed within 8 hr of collection. N_2O was determined by single-phase equilibration gas chromatography with electron capture detection similar to that described by Upstill-Goddard et al. (1996). Each individual sample was calibrated against three certified (±5%) reference standards of 287, 402, and 511 ppb (Air Products Ltd) which are traceable to NOAA WMO-N_2O-X2006A scale for N_2O mole fractions. Mean instrument precision from daily, triplicate analyses of the three calibration standards was <0.95% coefficient of variation. Concentrations of N_2O in seawater were calculated from solubility tables of Weiss and Price (1980) at equilibration temperature (~25°C) and salinity.

3. Results

3.1. Model Validation

The model skill in reproducing seasonal variability in vertical distributions of N_2O was assessed by comparing modeled saturations with measurement data collected in the Celtic Sea in November 2014 (Rees, 2019a), April 2015 (Rees, 2019b) and July 2015 (Rees & Stephens, 2019). Covering different seasons and extending
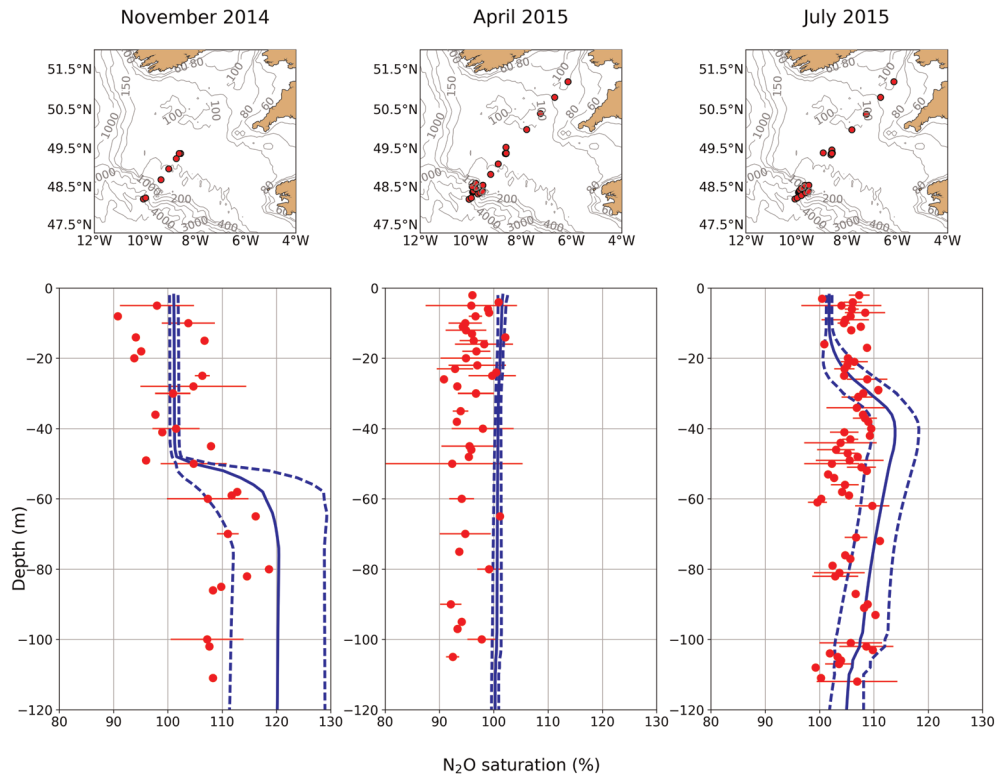
Figure 2. Comparison of modeled (solid lines) and measured (red dots) vertical profiles of N$_2$O saturation (%) in the Celtic Sea. Limits of standard deviation for modeled data are shown (dashed lines). For measurements, standard deviations are indicated if several measurements were taken at the same depth (horizontal lines). Maps (area denoted by red box on Figure 1) specify locations of stations sampled within each cruise.

geographically over a transect in the order of 600 km (Figure 2), these research expeditions captured contrasting conditions of the physical status and biological productivity of the shelf sea (e.g., García-Martín et al., 2019; Kitidis et al., 2017; Ruiz-Castillo et al., 2019).
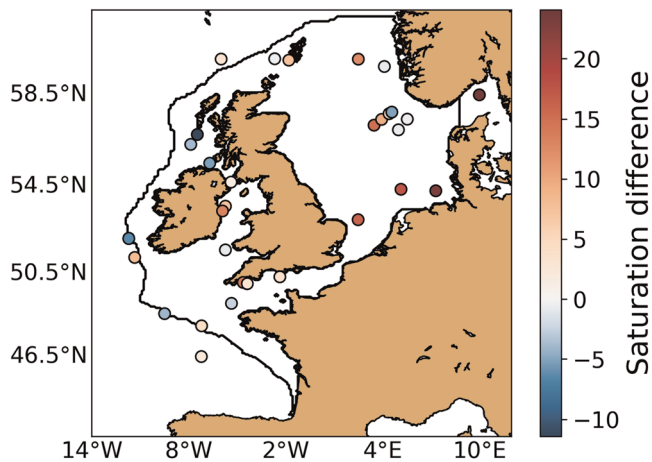

Figure 3. The difference between modeled and measured N$_2$O saturations (%) for June–July 2011, comparing measured values closest to the surface (<10 m depth) with corresponding results of the model. Positive (negative) values mean overestimation (underestimation) of N$_2$O saturations by the model.

Vertical profiles of N$_2$O saturations averaged over time and horizontal space were constructed for data collected within each of the three cruises and were compared with vertical profiles of modeled N$_2$O for the corresponding locations and time instances. During November 2014 (Figure 2, left), the model showed very low variability and vertically uniform saturations of N$_2$O close to equilibrium (about 101.2%) in the upper 50 m of the water column, and a pronounced increase in saturations between the depths of 50 and 70 m, up to about 120.2%. This increase was also evident in direct observations, though the model tends to slightly overestimate N$_2$O saturation at depths greater than 60 m. Vertically uniform N$_2$O saturations throughout water column were characteristic for the April 2015 (Figure 2, center), as shown both in the observational data and reproduced in the model, with the latter close to equilibrium, while the former mostly slightly undersaturated, with average saturations of 95.98% and 100.5% in the observations and in the model, respectively. For July 2015 (Figure 2, right), measurements showed N$_2$O saturations mostly between 100% and 110%. The model showed mean saturation of 101.8% in the upper 10 m, which increased to a maximum of 113.9% at 40 m depth, followed by a steady decrease with greater depth, bringing modeled results back into agreement with the observed values.
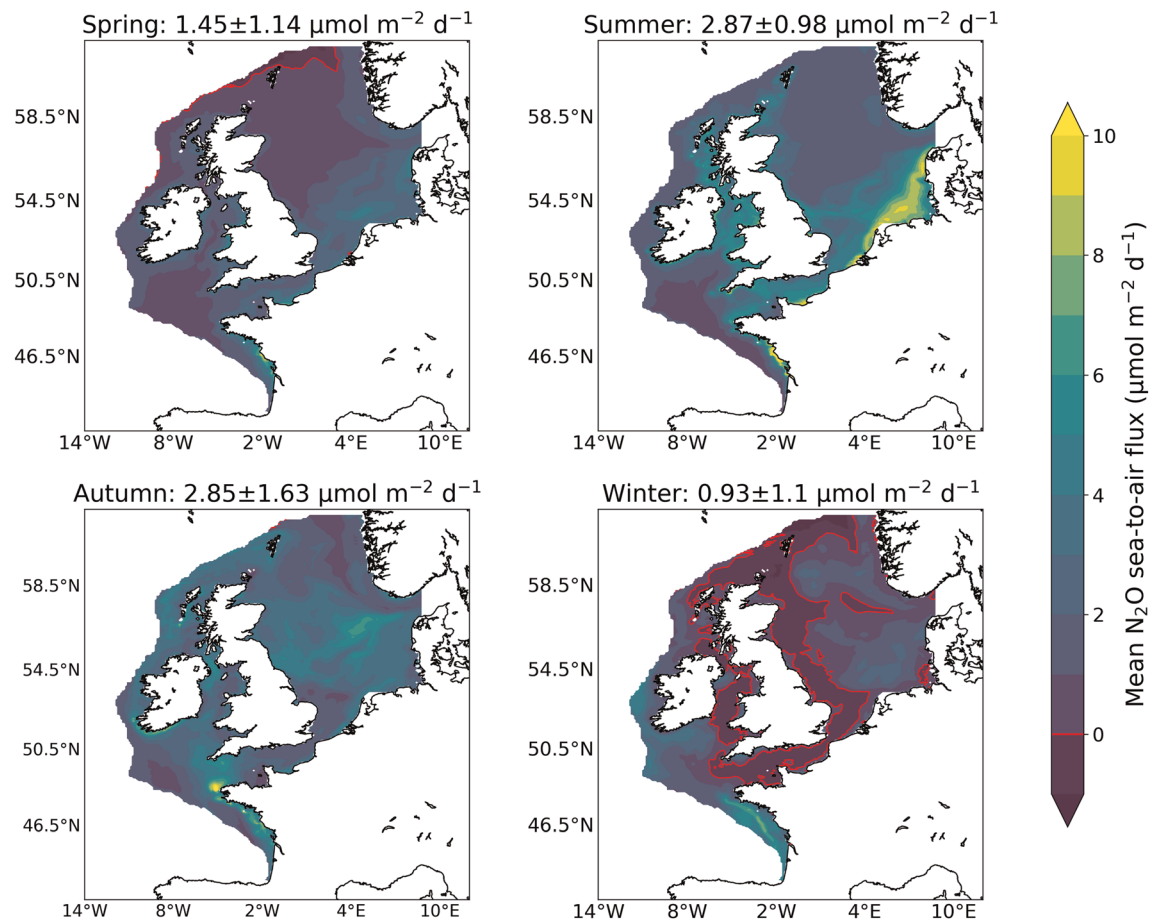
Figure 4. Seasonally averaged distribution of modeled N_2O air-sea fluxes ($\mu mol\ m^{-2}\ day^{-1}$) over the northwest European continental shelf based on a 2006–2015 climatology: Spring (March–May), summer (June–August), autumn (September–November), and winter (December–February). Positive values indicate outgassing of N_2O into the atmosphere, negative-uptake by the ocean. The red contour line separates regions with positive and negative fluxes.

The model skill in reproducing shelf-wide spatial distribution of N_2O saturations within surface waters was assessed by comparing model results with measurement data collected between June and July 2011 (Brown & Rees, 2014) (also available from the MEMENTO database; Bange et al., 2009; Kock & Bange, 2015), covering a range of geographical locations with varying hydrographical and biogeochemical conditions within the northwest European shelf (Figure 3). Measurements taken closest to the surface (where they were taken at depth < 10 m) were compared with the corresponding values from the model. Modeled saturations generally match measurements rather well, although there is a slight tendency for overestimation compared to observational data (modeled and measured saturations averaged over all stations are 107.36 ± 4.49% and 102.62 ± 6.75%, respectively). The overestimation is especially apparent for the highly productive shallow region in the southern North Sea, as well as Kattegat area.

3.2. Mean Seasonal Distributions of N_2O Air-Sea Fluxes

Characteristic seasonality of air-sea fluxes of N_2O over the northwest European continental shelf area (defined here as part of the modeled domain delineated with the 200 m isobath, but also including the Norwegian Trench) is assessed based on a climatological year representing the average of a 10-year model simulation (2006–2015).

The northwest European continental shelf as a whole is a source of N_2O to the atmosphere, emitting on average 2.03 ± 1.93 $\mu mol\ N_2O\ m^{-2}\ day^{-1}$. However, there is a considerable amount of variability in the distribution of fluxes between seasons, as well as spatial differences within each individual season (Figure 4).
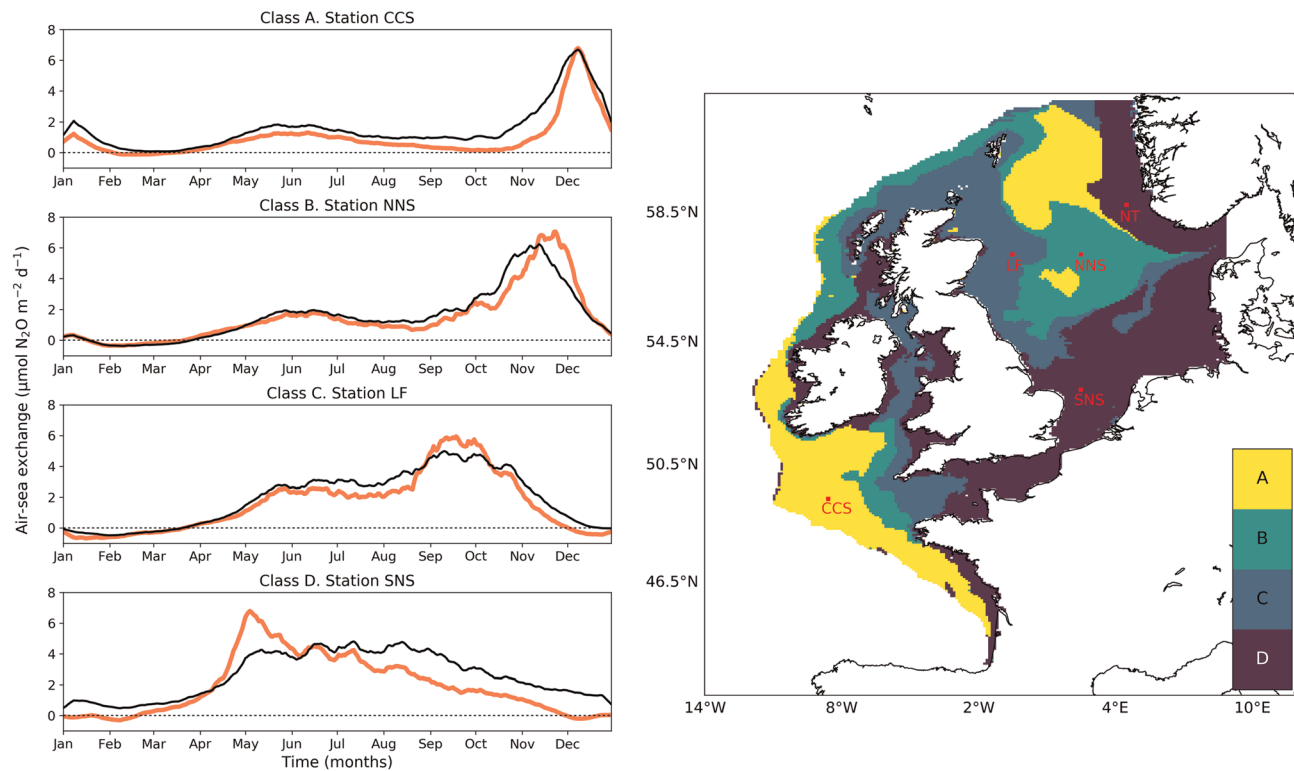
Figure 5. (left) Seasonal patterns of N$_2$O sea-to-air fluxes, mean over the region (black lines) and at selected stations (red lines). Positive values indicate outgassing to the atmosphere, negative-uptake. To remove weather-related noise, fluxes are shown as 14-day moving average values. (right) The corresponding spatial distribution of classes (A–D) within the northwest European continental shelf area. Location of stations CCS (Central Celtic Sea; 49.39°N,8.58°W), NNS (Northern North Sea; 57.25°W,2.5°E), LF (Long Forties area; 57.25°N,0.5°W), SNS (Southern North Sea; 53°N,2.5°E), and NT (Norwegian Trench; 58.75°W,4.5°E) are identified.

Fluxes to the atmosphere increase from spring toward summer, especially in the coastal areas around UK and the south-eastern North Sea region where maximum values rise from ~4 µmol m^{-2} day^{-1} in spring to ~10 µmol m^{-2} day^{-1} in summer. In autumn, in the North Sea, fluxes are comparatively higher offshore (reaching ~7 µmol m^{-2} day^{-1}) than in coastal regions. Fluxes are lower than in summer in the southernmost part of the North Sea and eastern English Channel, but higher in the western English Channel and eastern part of the Celtic Sea. Also in the northern shelf regions, N$_2$O outflux is greater in autumn than in summer. In winter, equilibrium conditions or weak negative fluxes (i.e., uptake of N$_2$O from the atmosphere) prevail over the western part of the North Sea, the English Channel and the Irish Sea. The rest of the area is characterized by low outgassing of <3 µmol m^{-2} day^{-1}, apart from a region west and southwest of Ireland (4–6 µmol m^{-2} day^{-1}) and along the western coast of France (up to 9 µmol m^{-2} day^{-1}).

3.3. Dominant Seasonal Patterns of N$_2$O Air-Sea Fluxes

Through the application of SOM, dominant classes (A–D) of seasonal cycle in N$_2$O air-sea fluxes on the northwest European shelf were identified (Figure 5, left). Class A is characterized by high fluxes during winter months (November–December), while low fluxes are typical for the rest of the year. Within classes B and C peak fluxes shift toward late-autumn (October–November) and early-autumn (September–October) months, respectively. For all the above classes, a minor increase in fluxes from early spring toward May–June is characteristic and consecutively more pronounced. Class D is characterized by bell-shaped seasonal distribution with higher fluxes from late spring until early autumn, peaking in summer (July–August), and low fluxes throughout winter months.

Spatially, seasonal distributions corresponding to class A are found within the southwestern region of our study area (Celtic Sea, outer part of Armorican shelf) and offshore region of the northern North Sea (Figure 5, right). Class B fluxes are characteristic for central North Sea and outer parts of Irish and

Shetland Shelves. Temporal patterns corresponding to class C can be found in the western English Channel, Irish Sea, coastward region of Shetland Shelf and western part of North Sea adjacent to UK coast. Class D represents south-eastern North Sea, central English Channel, coastal areas around UK, Ireland, and France, as well as Norwegian Trench.

4. Discussion

4.1. Controls of Seasonality in N_2O Air-Sea Fluxes

To determine the major drivers shaping the seasonal patterns of N_2O fluxes identified in the previous section, we have selected four stations within the model domain: CCS (Central Celtic Sea; 49.39°N,8.58°W), NNS (Northern North Sea; 57.25°W,2.5°E), LF (Long Forties area; 57.25°N,0.5°W), and SNS (Southern North Sea; 53°N,2.5°E), respectively representing classes A, B, C, and D (see Figure 5). Temporal patterns of air-sea fluxes of N_2O, as well as their absolute values at these stations rather well reflect the average-per-class values, showing short-lasting winter maximum for class A, bell-shaped seasonal distributions of class D (although with a maximum skewed toward late-spring period at SNS station), and classes B and C showing transitional dynamics between the former two (Figure 5, left).

The distinct seasonality of N_2O air-sea fluxes among these stations, and, therefore, between the identified regions, depends on the seasonality of N_2O saturation state within surface waters and the underlying mechanisms controlling it. Thus, the region corresponding to class A is characterized by relatively deep water and strong seasonal density stratification (Figure 6; Station CCS). Excess N_2O (i.e., saturation state >100%) builds up from late spring until late autumn below the seasonal pycnocline. Intrusion of these water masses, increasingly oversaturated with N_2O, into the upper mixed layer, is effectively prevented until the late autumn when stratification collapses and excess N_2O is allowed to escape into the atmosphere. A similar mechanism for the buildup of N_2O oversaturation exists within class B (Figure 6; Station NNS), which is also characterized by strong seasonal density stratification, albeit at shallower water depths. During the stratified period, oversaturation of N_2O builds up below, but also within the pycnocline. As the water column gradually starts to mix from September onward, this facilitates earlier outgassing of excess N_2O into the atmosphere relative to class A. For the region corresponding to class C (Figure 6; Station LF), more transient, weaker, and shorter-lasting water column stratification is typical. This allows for more effective outgassing during spring and summer compared to the previous two classes. Subsequently, mixing of the water column due to the earlier breakdown of stratification during September–October results in high fluxes of N_2O into the atmosphere, leaving water either at equilibrium or weakly undersaturated with respect to the atmosphere until the following spring (see Figure 5, left). Finally, class D is typically represented by shallow coastal areas and is characterized by a permanently mixed water column (Figure 6; Station SNS). Here, saturation of N_2O increases from spring (specifically, April in case of SNS station), and is maintained at relatively high levels throughout the summer months, eventually decreasing from late summer to early autumn.

Within temporally stratified regions (classes A and B), bulk N_2O production mostly takes place below the mixed layer, allowing for the gradual buildup of oversaturation (excess N_2O) below the pycnocline in waters isolated from the surface mixed layer and without contact with the atmosphere until stratification starts to break down (Figure 7; Stations CCS and NNS). However, in spring some N_2O production within these regions takes place at the base of mixed layer, fueling the concurrent increase in air-sea fluxes (see Figure 5 for the corresponding stations).

Within class C, when water column is mixed during spring-early summer and early autumn, N_2O production occurs uniformly throughout the water column (Figure 7; Station LF). Throughout the relatively short stratification period, excess N_2O builds up below the pycnocline, driving an increase in outflux to the atmosphere in early autumn (see Figure 5). Within permanently mixed regions corresponding to class D, lack of stratification allows for the excess N_2O to escape to the atmosphere as soon as it is produced (Figure 7; Station SNS). As a result of the SOM analysis, air-sea flux of N_2O within the Norwegian Trench was attributed to class D, otherwise characteristic for shallow permanently mixed regions. This is explained by a strong density gradient between ~20–30 m depth, leading to the bulk of N_2O production, followed by outgassing, to take place within the upper mixed layer during the productive season. This results in a temporal pattern of
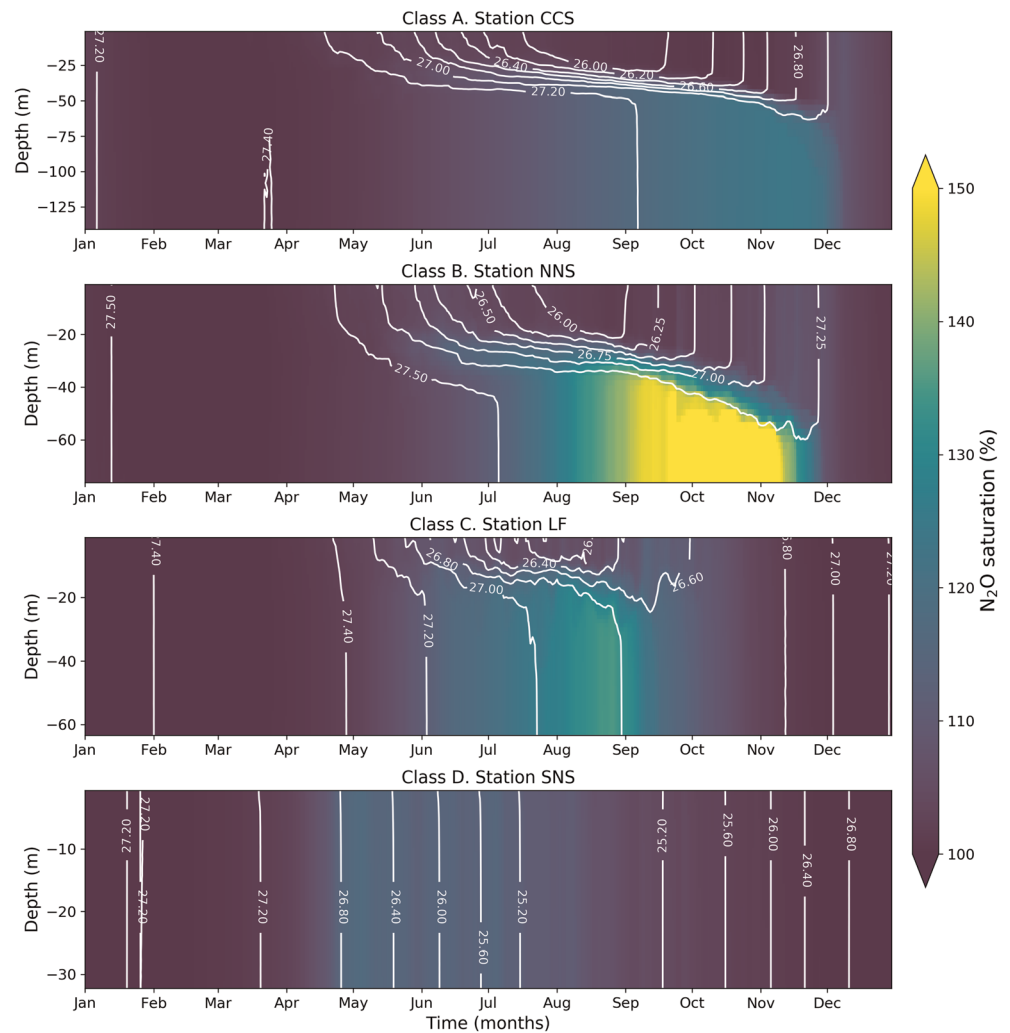
Figure 6. Seasonal distributions of N_2O saturations (%) over a climatological year (based on 2006–2015) at stations CCS (Central Celtic Sea; 49.39°N,8.58°W), NNS (Northern North Sea; 57.25°W,2.5°E), LF (Long Forties area; 57.25°N,0.5°W), and SNS (Southern North Sea; 53°N,2.5°E), representing classes A, B, C, and D, respectively. White contour lines indicate density anomaly (kg m^{-3}).

emissions showing lower rates during winter and higher fluxes in summer (Figure S1 in the supporting information).

4.2. The Northwest European Shelf as a Source of N_2O

By synthesizing observational evidence, Bange (2006) estimated mean N_2O saturations of 113% for the whole European shelf. Our results indicate a mean N_2O saturation of 104.9% for the northwest European continental shelf (Table 1), which is somewhat lower than Bange (2006) estimate which included the high contributions of the Baltic Sea and some areas of the Mediterranean. For the Central North Sea, Law and Owens (1990) reported saturations of 102.2%, while Bange et al. (1996) gave estimates of 104%, which are rather close to the mean given by our model results for classes B and C, representing the central North Sea region.

With the mean air-sea fluxes of $2.03 \pm 1.93\ \mu mol\ N_2O\ m^{-2}\ day^{-1}$, our model results show that the northwest European shelf N_2O emissions contribute 0.02224 Tg N yr^{-1} to the atmosphere. This comprises between 3.3% and 6.8% of the total emissions from European shelves and estuaries which are estimated to be 0.33–0.67 Tg N yr^{-1} (Bange, 2006). Almost half (49%) of the total emissions within our study area originate from productive coastal regions corresponding to class D; the highest fluxes occur during summer and autumn,
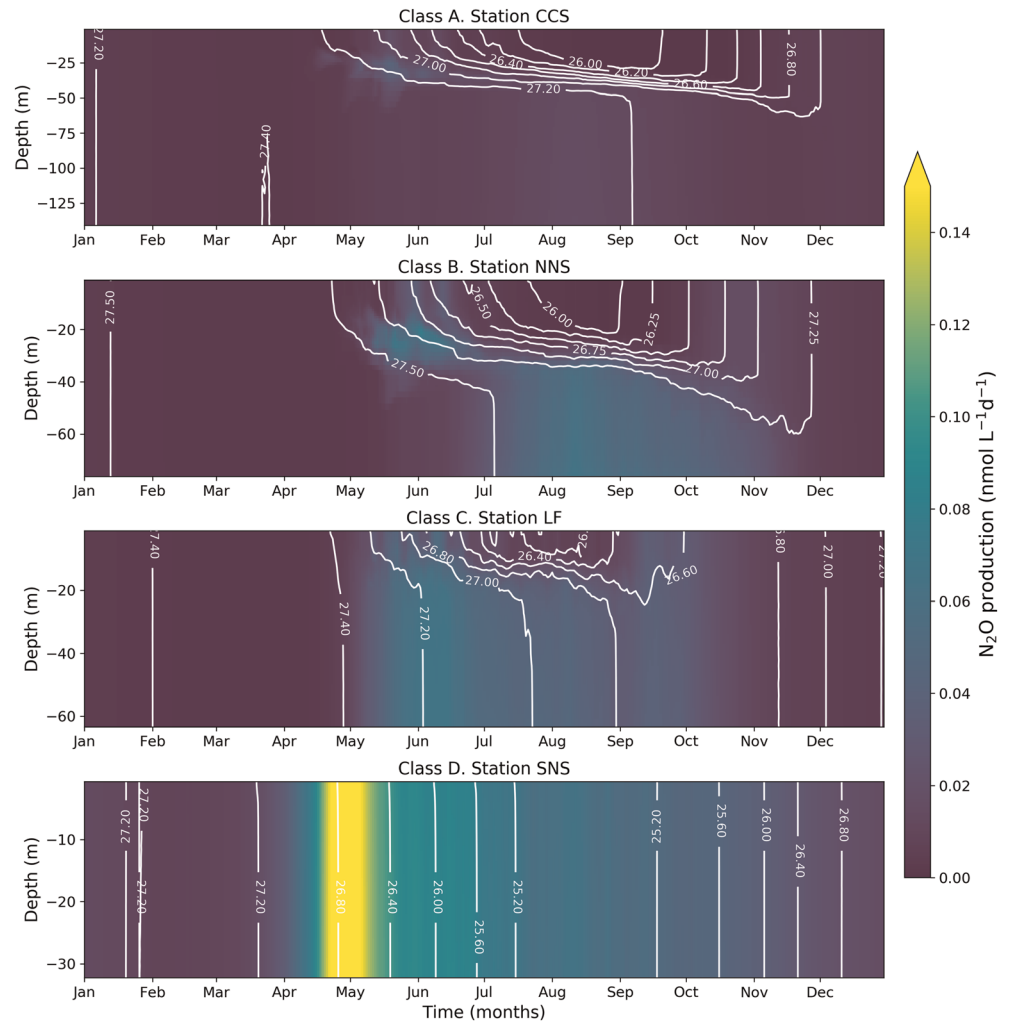
Figure 7. Seasonal distributions of N_2O production (nmol L^{-1} day^{-1}) over a climatological year (based on 2006–2015) at stations CCS (Central Celtic Sea; 49.39°N,8.58°W), NNS (Northern North Sea; 57.25°W,2.5°E), LF (Long Forties area; 57.25°N,0.5°W), and SNS (Southern North Sea; 53°N,2.5°E), representing classes A, B, C, and D, respectively. White contour lines indicate density anomaly (kg m^{-3}).

accounting for up to 71% of the total emissions (Table 1). Class D shows the highest emissions (0.00459 Tg N) in summer, regions of C and B classes in autumn (0.00206 and 0.00183 Tg N, respectively), and class A in winter (0.00138 Tg N), following the differences in intensity and duration of stratification among these classes (see Figure 5). Notably, in contrast to other regions and seasons, class C on average acts as a weak

Table 1
Modeled Daily Mean Air-Sea Fluxes (µmol N_2O m^{-2} day^{-1}), Saturations (%) and Total Emissions (Tg N per Season and per Year) From Regions Corresponding to the Identified Classes (A–D)

Region/class		A	B	C	D	Total
Mean saturation (%)		102.83 ± 2.25	102.86 ± 2.58	104.56 ± 4.54	107.21 ± 5.79	104.89 ± 4.16
Mean air-sea flux (µmol m^{-2} d^{-1})		1.57 ± 1.79	1.59 ± 1.93	1.87 ± 2.07	2.59 ± 1.93	2.03 ± 1.93
Total emission, (Tg N)	Spring	0.00052	0.00032	0.0006	0.00258	0.00401
	Summer	0.00077	0.00072	0.00185	0.00459	0.00794
	Autumn	0.00115	0.00183	0.00206	0.00275	0.00779
	Winter	0.00138	0.00024	−0.0001	0.00099	0.0025
	Total (y^{-1})	0.00382	0.00311	0.00441	0.01091	0.02224

sink for atmospheric N_2O in winter (see also Figure 4). Previous modeling work by Holt et al. (2012) has projected that a significant area of the northwest European shelf will become increasingly stratified under the influence of future climate. From the perspective of dynamics of N_2O fluxes, this is expected to lead to an expansion of class A and B regions in the future, with potential decrease in emissions within these regions due to decreased productivity. This will in turn lead to stronger decoupling from coastal regions which are less influenced by the open ocean processes, i.e. class C and D regions, where mixing is expected to intensify further, along with biogeochemical cycling enhanced by higher temperatures.

As part of its international commitments, the UK submits annual estimates of anthropogenic greenhouse gas emissions to the United Nations Framework Convention on Climate Change (UNFCCC) and the European Union Monitoring Mechanism Regulation (MMR). According to the UK National Atmospheric Emissions Inventory (NAEI, https://naei.beis.gov.uk/), total anthropogenic emissions from all sources within the UK comprise 0.04598 Tg N yr^{-1} on average for the period 2006–2015. Our study shows that the on-shelf part of the UK EEZ annually emits 0.00877 Tg N, a considerable addition of 19.1% to the total land-based emission estimates, and 29% compared to UK emissions from agricultural sources, which comprise 0.03027 Tg N yr^{-1}. Although N_2O is naturally produced within the marine environment and therefore is not included in the national accounting, anthropogenic nutrient input has the potential to increase emissions within coastal seas. Further regional modeling efforts are necessary to quantify the contribution of human activity to N_2O emissions from coastal regions and inform policy on their management potential, for example, via nutrient input reduction measures.

As is the case for the northwest European shelf as a whole, a substantial degree of heterogeneity in spatio-temporal distributions of emissions exists within the on-shelf part of the UK EEZ, as indicated by average air-sea flux of 1.7 ± 1.84 µmol m^{-2} day^{-1} and saturation of $104.4 \pm 3.86\%$. This variability highlights that more accurate measurement-based estimates of N_2O fluxes require higher temporal and spatial sampling resolution, which can be facilitated via the establishment of a harmonized N_2O Ocean Observation Network, as proposed by Bange et al. (2019). This initiative will support the development of models such as the one used in the current study, for further improvement of our understanding of the present dynamics and future trends in marine N_2O emissions.

4.3. Critical Assessment of Model Assumptions and the Future Outlook

The modeled N_2O air-sea flux values (Table 1) are prone to uncertainties in the adopted formulation and parameterization of N_2O production and air-sea exchange. For instance, the model overestimates N_2O percent saturation at water depths of ~40 m during summer (Figure 2, right), which potentially results in overestimated sea-to-air flux within temporally stratified regions. Nevertheless, since accumulation of N_2O in the water column and timing of its release to the atmosphere are controlled by the stratification regime, the reliable representation of seasonality depends on the accuracy of our hydrodynamic model simulations.

Our model formulation allows for the enhancement of N_2O production at low oxygen conditions. However, within this study the impact on production was negligible due to high oxygen content throughout the model domain (not shown). Our results thus indicate that N_2O production within the waters of northwest European shelf is primarily a function of substrate (ammonium) availability, and may be modified by temperature and pH variability (Beman et al., 2011; Huesemann et al., 2002; Kitidis et al., 2011) affecting nitrification rate, as parameterized in ERSEM (Butenschön et al., 2016).

As demonstrated by Zamora and Oschlies (2014), nitrification rates and the corresponding N_2O production within the surface ocean are the major sources of uncertainty for emission estimates within global model settings. Although in our model we did not explicitly limit nitrification (and hence N_2O production) within the photic zone, the model showed that most of the N_2O production within temporally stratified regions (classes A and B) occurs at the base of the pycnocline as it starts to develop in spring. During the remainder of the stratified period N_2O production continued below the pycnocline, with production rates within surface layers remaining very low both during stratified and mixed seasons. These distributions of production correlate with those of ammonium accumulation (Figure S2 in the supporting information). The model therefore suggests that lower nitrification in the photic zone is an emergent property related to the substrate dynamics rather than to photoinhibition. This complements the findings of Smith et al. (2014), who ascribed the competition between nitrifiers and phytoplankton for ammonium as the dominant factor limiting N_2O

production within the photic zone. In shallower, well-mixed regions (class D and, to some extent, class C) the supply of ammonium is abundant throughout water column, as is the production of N_2O, during the entire biologically active period. Nevertheless, the existing uncertainty surrounding the role of light in regulating nitrification rates creates an imperative for further modeling and experimental studies exploring the sensitivity of ammonia oxidation to different light levels and regimes, and its effects on the production of N_2O.

The model parameterization adopted in this paper focuses on nitrification as a single process generating N_2O, which, as we have demonstrated, is appropriate for the geographical region and the spatial resolution of the model used in this study. However, its application in areas experiencing lower oxygen concentrations (e.g., upwelling regions) or dynamic sediment activity (e.g., estuaries) requires more detailed consideration of the whole nitrogen cycle. This is particularly so with respect to the parameterization of denitrification within benthic and pelagic zones which may provide either a source or sink of N_2O. Future iterations should also consider the inclusion of anammox and dissimilatory nitrate reduction to ammonium (DNRA), which may affect the N_2O cycle by modifying substrate availability. The understanding of these processes, however, remains incomplete, which hinders their implementation within large-scale model simulations. For instance, there is evidence from terrestrial environments that some organisms responsible for DNRA can potentially consume N_2O (Sanford et al., 2012). The priority for future model development and its implementation within the northwest European shelf is an exploration of the model sensitivity to varied parameterizations of benthic N_2O sinks and sources, as this has the potential to increase model accuracy in biogeochemically complex productive shallow regions, where the model to data match is weaker (see Figure 3).

Observations of N_2O concentrations and air-sea exchange remain sparsely distributed both in space and in time, even for the northwest European shelf. Recent developments in technology for increasing the frequency of measurements (e.g., Grefe & Kaiser, 2014) coupled with improvements in flux estimation (e.g., Holding et al., 2019) and systematically coordinated observations (Bange et al., 2019; Wilson et al., 2018) will each contribute to refinements in the N_2O budget. In addition to the space- and time-resolving measurements of N_2O concentrations, model developments will require better constraints on the rates and distributions of nitrogen cycling processes over the estuarine-coastal-offshore continuum. The targeting of specific undefined processes, for example, the factors controlling the balance between anammox and denitrification (Kitidis et al., 2017) and the potential for N_2O consumption in oxygenated waters (e.g., Raes et al., 2016) remain a high priority in order to further our understanding of the extremely complex marine nitrogen cycle and thus to enable the mechanistic implementation of enigmatic processes into future model environment.

5. Conclusions

Within this study we have augmented a well-established biogeochemical-ecological model with N_2O-related processes to study distributions and controls of air-sea fluxes of this potent greenhouse gas within the northwest European continental shelf region.

Our study has shown that physical constraints directly regulate seasonal patterns of N_2O fluxes on the shelf. The duration and intensity of water column stratification defines the vertical position and timing of N_2O production. This, in turn, offers the control to the accumulation of excess N_2O within the water column and the timing and rate of subsequent release to the atmosphere. The physical regime and its inherent seasonal variability also regulate biological productivity which controls the supply of ammonium for nitrification via planktonic excretion and exudation, and via organic matter mineralization, and determines the total amount of N_2O produced and eventually lost to the atmosphere.

We estimate that the northwest European shelf as a whole is a source of N_2O to the atmosphere, contributing 0.02224 Tg N annually, which, however, comprises only between 3.3 and 6.8% of total emissions from European shelves and estuaries. Since 49% of the total emissions within our study area originate from coastal regions, changes in anthropogenic nutrient input have the potential to substantially impact on regional N_2O emissions. Further modeling efforts will quantify the anthropogenic footprint of these emissions and project their future changes.

References

Andreae, M. O., & Crutzen, P. J. (1997). Atmospheric aerosols: Biogeochemical sources and role in atmospheric chemistry. *Science*, *276*(5315), 1052–1058. https://doi.org/10.1126/science.276.5315.1052

Bange, H. W. (2006). Nitrous oxide and methane in European coastal waters. *Estuarine, Coastal and Shelf Science*, *70*(3), 361–374.

Bange, H. W. (2008). Gaseous nitrogen compounds (NO, N_2O, N_2, NH_3) in the ocean. In D. G. B. Capone, M. R. Mulholland, & E. J. Carpenter (Eds.), *Nitrogen in the marine environment*, (pp. 51–94). Amsterdam: Elsevier.

Bange, H. W., Arévalo-Martínez, D. L., de la Paz, M., Farías, L., Kaiser, J., Kock, A., et al. (2019). A harmonized nitrous oxide (N_2O) ocean observation network for the 21st century. *Frontiers in Marine Science*, *6*(157). https://doi.org/10.3389/fmars.2019.00157

Bange, H. W., Bell, T. G., Cornejo, M., Freing, A., Uher, G., Upstill-Goddard, R. C., & Zhang, G. (2009). MEMENTO: A proposal to develop a database of marine nitrous oxide and methane measurements. *Environmental Chemistry*, *6*(3), 195–197.

Bange, H. W., Rapsomanikis, S., & Andreae, M. O. (1996). Nitrous oxide in coastal waters. *Global Biogeochemical Cycles*, *10*(1), 197–207. https://doi.org/10.1029/95GB03834

Battaglia, G., & Joos, F. (2018). Marine N_2O emissions from nitrification and denitrification constrained by modern observations and projected in multimillennial global warming simulations. *Global Biogeochemical Cycles*, *32*, 92–121. https://doi.org/10.1002/2017gb005671

Beman, J. M., Chow, C. E., King, A. L., Feng, Y., Fuhrman, J. A., Andersson, A., et al. (2011). Global declines in oceanic nitrification rates as a consequence of ocean acidification. *Proceedings of the National Academy of Sciences*, *108*(1), 208–213.

Beman, M. J., Popp, B. N., & Alford, S. E. (2012). Quantification of ammonia oxidation rates and ammonia-oxidizing archaea and bacteria at high resolution in the Gulf of California and eastern tropical North Pacific Ocean. *Limnology and Oceanography*, *57*(3), 711–726. https://doi.org/10.4319/lo.2012.57.3.0711

Bianchi, D., Dunne, J. P., Sarmiento, J. L., & Galbraith, E. D. (2012). Data-based estimates of suboxia, denitrification, and N_2O production in the ocean and their sensitivities to dissolved O2. *Global Biogeochemical Cycles*, *26*, GB2009. https://doi.org/10.1029/2011gb004209

Blackford, J. C., Allen, J. I., & Gilbert, F. J. (2004). Ecosystem dynamics at six contrasting sites: A generic modelling study. *Journal of Marine Systems*, *52*(1), 191–215. https://doi.org/10.1016/j.jmarsys.2004.02.004

Blackford, J. C., & Gilbert, F. J. (2007). pH variability and CO_2 induced acidification in the North Sea. *Journal of Marine Systems*, *64*(1), 229–241. https://doi.org/10.1016/j.jmarsys.2006.03.016

Brown, I., and A. Rees (2014), UKOA D366 dissolved methane (CH_4) and nitrous oxide (N_2O) concentrations from CTD bottle samples, edited, British Oceanographic Data Centre - Natural Environment Research Council, UK, https://doi.org/10.5285/fd3287f9-f327-7f48-e043-6c86abc09b63

Bruggeman, J., & Bolding, K. (2014). A general framework for aquatic biogeochemical models. *Environmental Modelling and Software*, *61*(C), 249–265. https://doi.org/10.1016/j.envsoft.2014.04.002

Butenschön, M., Clark, J., Aldridge, J. N., Allen, J. I., Artioli, Y., Blackford, J., et al. (2016). ERSEM 15.06: A generic model for marine biogeochemistry and the ecosystem dynamics of the lower trophic levels. *Geoscientific Model Development*, *9*(4), 1293–1339. https://doi.org/10.5194/gmd-9-1293-2016

Capone, D. G. (1991), Aspects of the marine nitrogen cycle with relevance to the dynamics of nitrous and nitric oxide, Microbial production and consumption of greenhouse gases: Methane, nitrogen oxides, and halomethanes, 255–275.

Carpenter, L. J., Reimann, S., Burkholder, J. B., Clerbaux, C., Hall, B. D., Hossaini, R., et al. (2014). Update on ozone-depleting substances (ODSs) and other gases of interest to the Montreal protocol. *Scientific Assessment Of Ozone Depletion*, *2014*, 1.1–1.101.

Ciais, P., Sabine, C., Bala, G., Bopp, L., Brovkin, V., Canadell, J., et al. (2013). Carbon and other biogeochemical cycles. In T. F. Stocker, D. Qin, G.-K. Plattner, M. Tignor, S. K. Allen, J. Boschung, A. Nauels, Y. Xia, V. Bex, & P. M. Midgley (Eds.), *Climate change 2013: The physical science basis. Contribution of Working Group I to the Fifth Assessment Report of the Intergovernmental Panel on Climate Change* (pp. 465–570). Cambridge, United Kingdom and New York, NY, USA: Cambridge University Press. https://doi.org/10.1017/CBO9781107415324.015

Clark, D. R., Rees, A. P., & Joint, I. (2008). Ammonium regeneration and nitrification rates in the oligotrophic Atlantic Ocean: Implications for new production estimates. *Limnology and Oceanography*, *53*(1), 52–62.

Codispoti, L. A. (2010). Interesting times for marine N_2O. *Science*, *327*(5971), 1339–1340. https://doi.org/10.1126/science.1184945

Cohen, Y., & Gordon, L. I. (1978). Nitrous oxide in the oxygen minimum of the eastern tropical North Pacific: Evidence for its consumption during denitrification and possible mechanisms for its production. *Deep Sea Research*, *25*(6), 509–524. https://doi.org/10.1016/0146-6291(78)90640-9

Dee, D. P., Uppala, S. M., Simmons, A. J., Berrisford, P., Poli, P., Koyabashi, S. et al. (2011). The ERA-interim reanalysis: Configuration and performance of the data assimilation system. *Quarterly Journal of the Royal Meteorological Society*, *137*(656), 553–597. https://doi.org/10.1002/qj.828

Dore, J. E., & Karl, D. M. (1996). Nitrification in the euphotic zone as a source for nitrite, nitrate, and nitrous oxide at station ALOHA. *Limnology and Oceanography*, *41*(8), 1619–1628.

Edwards, K. P., Barciela, R., & Butenschön, M. (2012). Validation of the NEMO-ERSEM operational ecosystem model for the north west European continental shelf. *Ocean Science*, *8*(6), 983–1000. https://doi.org/10.5194/os-8-983-2012

Ferry, N., et al. (2012). GLORYS2V1 global ocean reanalysis of the altimetric era (1992-2009) at meso scale. *Mercator Quarterly Newsletter*, *44*, 29–39.

Freing, A., Wallace, D. W. R., & Bange, H. W. (2012). Global oceanic production of nitrous oxide. *Philosophical Transactions of the Royal Society, B: Biological Sciences*, *367*(1593), 1245–1255. https://doi.org/10.1098/rstb.2011.0360

García-Martín, E. E., Daniels, C. J., Davidson, K., Davis, C. E., Mahaffey, C., Mayers, K. M. J., et al. (2019). Seasonal changes in plankton respiration and bacterial metabolism in a temperate shelf sea. *Progress in Oceanography*, *177*, 101884. https://doi.org/10.1016/j.pocean.2017.12.002

Goreau, T. J., Kaplan, W. A., Wofsy, S. C., McElroy, M. B., Valois, F. W., & Watson, S. W. (1980). Production of NO_2^- and N_2O by nitrifying bacteria at reduced concentrations of oxygen. *Applied and Environmental Microbiology*, *40*(3), 526–532.

Grefe, I., & Kaiser, J. (2014). Equilibrator-based measurements of dissolved nitrous oxide in the surface ocean using an integrated cavity output laser absorption spectrometer. *Ocean Science*, *10*(3), 501–512. https://doi.org/10.5194/os-10-501-2014

Holding, T., Ashton, I. G., Shutler, J. D., Land, P. E., Nightingale, P. D., Rees, A. P., et al. (2019). The FluxEngine air–sea gas flux toolbox: Simplified interface and extensions for in situ analyses and multiple sparingly soluble gases. *Ocean Science*, *15*(6), 1707–1728. https://doi.org/10.5194/os-15-1707-2019

Holt, J., Butenschön, M., Wakelin, S. L., Artioli, Y., & Allen, J. I. (2012). Oceanic controls on the primary production of the northwest European continental shelf: Model experiments under recent past conditions and a potential future scenario. *Biogeosciences*, *9*(1), 97–117. https://doi.org/10.5194/bg-9-97-2012

Holt, J., Hyder, P., Ashworth, M., Harle, J., Hewitt, H. T., Liu, H., et al. (2017). Prospects for improving the representation of coastal and shelf seas in global ocean models. *Geoscientific Model Development*, *10*(1), 499–523. https://doi.org/10.5194/gmd-10-499-2017

Horak, R. E. A., Qin, W., Bertagnolli, A. D., Nelson, A., Heal, K. R., Han, H. et al. (2018). Relative impacts of light, temperature, and reactive oxygen on thaumarchaeal ammonia oxidation in the North Pacific Ocean. *Limnology and Oceanography*, *63*(2), 741–757. https://doi.org/10.1002/lno.10665

Horrigan, S., & Springer, A. (1990). Oceanic and estuarine ammonium oxidation: Effects of light. *Limnology and Oceanography*, *35*(2), 479–482.

Huesemann, M. H., Skillman, A. D., & Crecelius, E. A. (2002). The inhibition of marine nitrification by ocean disposal of carbon dioxide. *Marine Pollution Bulletin*, *44*(2), 142–148. https://doi.org/10.1016/S0025-326X(01)00194-1

Hyder, K., Rossberg, A. G., Allen, J. I., Austen, M. C., Barciela, R. M., Bannister, H. J., et al. (2015). Making modelling count—Increasing the contribution of shelf-seas community and ecosystem models to policy development and management. *Marine Policy*, *61*, 291–302. https://doi.org/10.1016/j.marpol.2015.07.015

IPCC (2013). *Climate change 2013: The physical science basis. Contribution of Working Group I to the Fifth Assessment Report of the Intergovernmental Panel on Climate Change* (p. 1535). Cambridge, United Kingdom and New York, NY, USA: Cambridge University press. https://doi.org/10.1017/CBO9781107415324

Ji, Q., Buitenhuis, E., Suntharalingam, P., Sarmiento, J. L., & Ward, B. B. (2018). Global nitrous oxide production determined by oxygen sensitivity of nitrification and denitrification. *Global Biogeochemical Cycles*, *32*, 1790–1802. https://doi.org/10.1029/2018gb005887

Kitidis, V., Laverock, B., McNeill, L. C., Beesley, A., Cummings, D., Tait, K., et al. (2011). Impact of ocean acidification on benthic and water column ammonia oxidation. *Geophysical Research Letters*, *38*, L21603. https://doi.org/10.1029/2011gl049095

Kitidis, V., Tait, K., Nunes, J., Brown, I., Woodward, E., Harris, C., et al. (2017). Seasonal benthic nitrogen cycling in a temperate shelf sea: The Celtic Sea. *Biogeochemistry*, 1-17.

Kock, A., & Bange, H. W. (2015). Counting the ocean's greenhouse gas emissions. *Eos*, *96*(3), 10–13.

Kohonen, T. (2001). *Self-organizing maps*. Berlin Heidelberg: Springer.

Law, C. S., & Owens, N. J. P. (1990). Denitrification and nitrous oxide in the North Sea. *Netherlands Journal of Sea Research*, *25*(1), 65–74. https://doi.org/10.1016/0077-7579(90)90009-6

Löscher, C. R., Kock, A., Könneke, M., LaRoche, J., Bange, H. W., & Schmitz, R. A. (2012). Production of oceanic nitrous oxide by ammonia-oxidizing archaea. *Biogeosciences*, *9*(7), 2419–2429. https://doi.org/10.5194/bg-9-2419-2012

Martinez-Rey, J., Bopp, L., Gehlen, M., Tagliabue, A., & Gruber, N. (2015). Projections of oceanic N_2O emissions in the 21st century using the IPSL earth system model. *Biogeosciences (BG)*, *12*(13), 4133–4148.

Merbt, S. N., Stahl, D. A., Casamayor, E. O., Martí, E., Nicol, G. W., & Prosser, J. I. (2012). Differential photoinhibition of bacterial and archaeal ammonia oxidation. *FEMS Microbiology Letters*, *327*(1), 41–46. https://doi.org/10.1111/j.1574-6968.2011.02457.x

Myhre, G., Shindell, D., Bréon, F.-M., Collins, W., Fuglestvedt, J., Huang, J., et al. (2013). Climate change 2013: The physical science basis. In M. Tignor, S. K. Allen, J. Boschung, et al. (Eds.), *Contribution of working group I to the fifth assessment report of the intergovernmental panel on climate change* (pp. 659–740). Cambridge, United Kingdom and New York, NY, USA: Cambridge University Press. https://doi.org/10.1017/CBO9781107415324.018

Nevison, C., Butler, J. H., & Elkins, J. W. (2003). Global distribution of N_2O and the ΔN_2O-AOU yield in the subsurface ocean. *Global Biogeochemical Cycles*, *17*(4), 1119. https://doi.org/10.1029/2003gb002068

Nevison, C., & Holland, E. (1997). A reexamination of the impact of anthropogenically fixed nitrogen on atmospheric N_2O and the stratospheric O_3 layer. *Journal of Geophysical Research*, *102*(D21), 25,519–25,536. https://doi.org/10.1029/97JD02391

Newell, S. E., Fawcett, S. E., & Ward, B. B. (2013). Depth distribution of ammonia oxidation rates and ammonia-oxidizer community composition in the Sargasso Sea. *Limnology and Oceanography*, *58*(4), 1491–1500. https://doi.org/10.4319/lo.2013.58.4.1491

NOAA (2014). Combined nitrous oxide data from the NOAA/ESRL global monitoring division edited.

Peng, X., Fuchsman, C. A., Jayakumar, A., Warner, M. J., Devol, A. H., & Ward, B. B. (2016). Revisiting nitrification in the eastern tropical South Pacific: A focus on controls. *Journal of Geophysical Research: Oceans*, *121*, 1667–1684. https://doi.org/10.1002/2015jc011455

Raes, E. J., Bodrossy, L., van de Kamp, J., Holmes, B., Hardman-Mountford, N., Thompson, P. A., et al. (2016). Reduction of the powerful greenhouse gas N_2O in the south-eastern Indian Ocean. *PLoS ONE*, *11*(1), e0145996. https://doi.org/10.1371/journal.pone.0145996

Ravishankara, A. R., Daniel, J. S., & Portmann, R. W. (2009). Nitrous oxide (N_2O): The dominant ozone-depleting substance emitted in the 21st century. *Science*, *326*(5949), 123–125. https://doi.org/10.1126/science.1176985

Rees, A. (2019a). Dissolved nitrous oxide and methane in water column and pore water surface sediment (box corer) for UK Shelf Sea biogeochemistry cruise DY018, edited. U.K.: British Oceanographic Data Centre-Natural Environment Research Counci. doi:10/c2jf.

Rees, A. (2019b). Dissolved nitrous oxide in water column for UK Shelf Sea Biogeochemistry cruise DY019, edited. U.K.: British Oceanographic Data Centre - Natural Environment Research Council. doi:10/c2jg.

Rees, A., & Stephens, N. (2019). Dissolved nitrous oxide in water column for UK Shelf Sea Biogeochemistry cruise DY033, edited. U.K.: British Oceanographic Data Centre - Natural Environment Research Council. doi:10/c2jh.

Ruiz-Castillo, E., Sharples, J., Hopkins, J., & Woodward, M. (2019). Seasonality in the cross-shelf physical structure of a temperate shelf sea and the implications for nitrate supply. *Progress in Oceanography*, *177*, 101985. https://doi.org/10.1016/j.pocean.2018.07.006

Sanford, R. A., Wagner, D. D., Wu, Q., Chee-Sanford, J. C., Thomas, S. H., Cruz-García, C., et al. (2012). Unexpected nondenitrifier nitrous oxide reductase gene diversity and abundance in soils. *Proceedings of the National Academy of Sciences*, *109*(48), 19,709–19,714.

Smith, J. M., Chavez, F. P., & Francis, C. A. (2014). Ammonium uptake by phytoplankton regulates nitrification in the Sunlit Ocean. *PLoS ONE*, *9*(9), e108173. https://doi.org/10.1371/journal.pone.0108173

Suntharalingam, P., & Sarmiento, J. (2000). Factors governing the oceanic nitrous oxide distribution: Simulations with an ocean general circulation model. *Global Biogeochemical Cycles*, *14*(1), 429–454.

Suntharalingam, P., Sarmiento, J. L., & Toggweiler, J. R. (2000). Global significance of nitrous-oxide production and transport from oceanic low-oxygen zones: A modeling study. *Global Biogeochemical Cycles*, *14*(4), 1353–1370. https://doi.org/10.1029/1999GB900100

Upstill-Goddard, R. C., Rees, A. P., & Owens, N. J. P. (1996). Simultaneous high-precision measurements of methane and nitrous oxide in water and seawater by single phase equilibration gas chromatography. *Deep Sea Research Part I: Oceanographic Research Papers*, *43*(10), 1669–1682. https://doi.org/10.1016/S0967-0637(96)00074-X

Vettigli, G. (2019). MiniSom: Minimalistic and NumPybased implementation of the self organizing map, Edited.

Wankel, S. D., Kendall, C., Pennington, J. T., Chavez, F. P., & Paytan, A. (2007). Nitrification in the euphotic zone as evidenced by nitrate dual isotopic composition: Observations from Monterey Bay, California. *Global Biogeochemical Cycles*, *21*, GB2006. https://doi.org/10.1029/2006GB002723

Wanninkhof, R. (1992). Relationship between wind speed and gas exchange over the ocean. *Journal of Geophysical Research*, *97*(C5), 7373–7382.

Ward, B., Olson, R. J., & Perry, M. J. (1982). Microbial nitrification rates in the primary nitrite maximum off southern California. *Deep Sea Research Part A. Oceanographic Research Papers*, *29*(2), 247–255.

Ward, B. B. (2008). Chapter 5 - nitrification in marine systems. In D. G. Capone, D. A. Bronk, M. R. Mulholland, & E. J. Carpenter (Eds.), *Nitrogen in the marine environment (second edition)* (pp. 199–261). San Diego: Academic Press. https://doi.org/10.1016/B978-0-12-372522-6.00005-0

Weiss, R., & Price, B. (1980). Nitrous oxide solubility in water and seawater. *Marine Chemistry*, *8*(4), 347–359.

Wilson, S. T., Bange, H. W., Arévalo-Martínez, D. L., Barnes, J., Borges, A. V., Brown, I., et al. (2018). An intercomparison of oceanic methane and nitrous oxide measurements. *Biogeosciences*, *15*(19), 5891–5907. https://doi.org/10.5194/bg-15-5891-2018

Yool, A., Martin, A. P., Fernández, C., & Clark, D. R. (2007). The significance of nitrification for oceanic new production. *Nature*, *447*(7147), 999–1002. https://doi.org/10.1038/nature05885, https://www.nature.com/articles/nature05885#supplementary-information

Zamora, L. M., & Oschlies, A. (2014). Surface nitrification: A major uncertainty in marine N_2O emissions. *Geophysical Research Letters*, *41*, 4247–4253. https://doi.org/10.1002/2014GL060556